Numerical Analysis of Resistive Interchange Mode in Equilibria Consistent with Static Magnetic Islands in a Straight Heliotron Configuration

Kinya SAITO[1,a)], Katsuji ICHIGUCHI[1,2] and Ryuichi ISHIZAKI[1,2]

[1)]*The Graduate University for Advanced Studies, Toki, Gifu 509-5292, Japan*
[2)]*National Institute for Fusion Science, Toki, Gifu 509-5292, Japan*

Effects of a static magnetic island generated by an external magnetic field on the linear stability and the nonlinear dynamics of resistive interchange modes are numerically studied by means of the reduced magnetohydrodynamic (MHD) equations in a straight heliotron configuration. Equilibria consistent with the static magnetic island are examined, where the pressure profile is locally flat inside the separatrix. The linear growth rate of the interchange mode is decreased with the increase of the static island width. The mode is completely stabilized when the static island width exceeds a threshold value. The threshold width is almost the same as the half-width of the eigenfunction of the stream function obtained for the equilibrium without the static island. The saturation level of the kinetic energy in the nonlinear evolution is also decreased with the increase of the static island width. The island width and the pressure profile are also affected by the nonlinear saturation of the interchange mode.

1. Introduction

Resonant magnetic perturbations (RMPs) are now focused on the collapse control in the magnetic confinement of the fusion plasmas. The reduction of the pressure gradient due to the imposition of the RMPs is considered to have a potential to stabilize pressure driven modes. The confirmation of such stabilization effects is extensively carried out in many experiments. In tokamaks, the control of the edge localized modes with the RMPs has been widely examined for the purpose of the application to ITER [1]. Also in heliotrons, the stabilizing effects of the RMPs on the interchange modes are examined. Yamada *et al.* [2] studied the effects of the $(m, n) = (1, 1)$ RMP to the plasma in the Large Helical Device (LHD) [3], where m and n are the poloidal and the toroidal mode numbers, respectively. They observed that the fluctuation amplitude is reduced as the amplitude of the RMP increases and the fluctuation is completely suppressed when a sufficiently large RMP is imposed.

On the other hand, in the heliotron configurations, the interaction between the islands induced by the RMP and the interchange mode has also been studied with numerical calculations. Unemura *et al.* [4] analyzed the nonlinear evolution of the mode with static islands and obtained a pressure collapse. Garcia *et al.* [5, 6] studied the behavior of the magnetic islands including a diamagnetic effect and

showed an island oscillation due to the diamagnetic flow. Saito *et al.* [7, 8] examined the change of the width and the phase of the islands in the nonlinear evolution of the interchange modes and found that the island width is enlarged by the mode. Nishimura *et al.* also studied the interaction between the RMPs and the plasma flow in tokamaks and heliotrons [9–11]. All these studies treated equilibrium pressure profiles corresponding to nested flux surfaces and incorporated the RMPs by imposing a constant perturbed poloidal magnetic flux at the plasma boundary. In general, however, the equilibrium pressure profile is locally deformed by the existence of the static magnetic island. Therefore, the equilibrium pressure in the previous studies was not consistent with the geometry of the magnetic islands. Furthermore, the contribution of the local deformation of the pressure profile due to the existence of the islands to the behavior of the interchange modes was not taken into account. No systematic stability study of the interchange mode has been performed for equilibria with pressure profile consistent with the static magnetic islands.

Thus, in the present work, we analyze numerically the behavior of the interchange mode in the equilibria consistent with the island structure. To understand the fundamental physics, we investigate the interaction between the mode and the static island with the same mode numbers, $(m, n) = (1, 1)$ in a straight heliotron configuration. We utilize the reduced MHD equations [12] because the equations are useful for the analysis of such low mode number physics. As mentioned above, the equilibria consis-

author's e-mail: ichiguch@nifs.ac.jp

[a)] Present address: Numerical Flow Designing, CO., LTD. Shinagawa-ku, Tokyo 141-0022, Japan

tent with the static island are necessary for this analysis. To obtain such equilibria, we have developed the FLEC code [13, 14]. This code gives equilibrium solutions corresponding to the reduced MHD equations for a given finite RMP, of which the resultant pressure profile is locally flat inside the separatrix.

By using the code, we can obtain two kinds of the equilibrium solutions with local flat pressure profile inside the separatrix [13, 14]. The difference of the solutions depends on the continuity of the pressure gradient at the separatrix except the X-point. When the pressure gradient at the separatrix is required to be continuous, the equilibrium pressure gradient has to be zero at the X-point. On the other hand, when the pressure gradient at the separatrix is allowed to be discontinuous, the equilibrium pressure gradient can be finite at the X-point. In the former case, the region with the flat pressure profile is almost annular. Ichiguchi *et al.* [15, 16] already studied the stability contribution of such annular flat structure on the interchange mode and found that the structure stabilizes the mode effectively. Therefore, we examine the stability of the latter equilibrium with a finite gradient at the X-point to obtain the stabilizing effect of the static island in this paper. In the stability analysis, the NORM code [17] is utilized, which solves the reduced MHD equations. Since the original NORM code was developed only for the analysis of the equilibria with nested flux surfaces, we modify the code so as to treat the equilibrium with static islands. We follow the time evolution of the perturbation to obtain the linear growth rate and the nonlinear saturation level of the interchange mode. We also examine the changes in the width and the phase of the island and the pressure profile in the nonlinear evolution of the mode.

This paper is organized as follows. In Sec. 2, the reduced MHD equations used in the present study are explained. In Sec. 3, the equilibria consistent with the $(m, n) = (1, 1)$ static island calculated with the FLEC code are shown. The linear stability of the equilibria is also discussed. In Sec. 4, the nonlinear evolution of the interchange mode is considered. The saturation level of the kinetic energy and the behavior of the magnetic island and the pressure profile are discussed. Conclusions are given in Sec. 5.

2. Basic Equations

The effect of the static island with the mode numbers of $(m, n) = (1, 1)$ on the interchange mode with the same mode number is investigated in the present study. The reduced MHD equations [12] are utilized for the analysis in the cylindrical coordinates (r, θ, z), which are solved by the NORM code [17]. The equations are composed of the Ohm's law, the vorticity equation and the pressure equation for the poloidal flux $\Psi(r, \theta, z)$, the stream function $\Phi(r, \theta, z)$ and the plasma pressure $P(r, \theta, z)$. The normalized equations are given by

$$\frac{\partial \tilde{\Psi}}{\partial t} = -\boldsymbol{B}_{\mathrm{eq}} \cdot \nabla \tilde{\Phi} - \tilde{\boldsymbol{B}} \cdot \nabla \tilde{\Phi} + \frac{1}{S} \tilde{J}_z, \tag{1}$$

$$\frac{\mathrm{d} \tilde{U}}{\mathrm{d} t} = -\boldsymbol{B}_{\mathrm{eq}} \cdot \nabla \tilde{J}z - \tilde{\boldsymbol{B}} \cdot \nabla (Jz_{\mathrm{eq}} + \tilde{J}z)$$
$$+ \frac{1}{2\epsilon^2} \nabla \Omega \times \nabla \tilde{P} \cdot z + \nu \nabla_{\perp}^2 \tilde{U}, \tag{2}$$

and

$$\frac{\partial \tilde{P}}{\partial t} = z \times \nabla \tilde{\Phi} \cdot \nabla (P_{\mathrm{eq}} + \tilde{P}) + \kappa_{\perp} \nabla_{\perp}^2 \tilde{P}$$
$$+ \kappa_{\parallel} \{ (\boldsymbol{B}_{\mathrm{eq}} \cdot \nabla)(\boldsymbol{B}_{\mathrm{eq}} \cdot \nabla) \tilde{P} + (\boldsymbol{B}_{\mathrm{eq}} \cdot \nabla)(\tilde{\boldsymbol{B}} \cdot \nabla)(P_{\mathrm{eq}} + \tilde{P})$$
$$+ (\tilde{\boldsymbol{B}} \cdot \nabla)(\boldsymbol{B}_{\mathrm{eq}} \cdot \nabla) \tilde{P} + (\tilde{\boldsymbol{B}} \cdot \nabla)(\tilde{\boldsymbol{B}} \cdot \nabla)(P_{\mathrm{eq}} + \tilde{P}) \}. \tag{3}$$

Here, 'eq' and '$\sim$' refer the equilibrium and the perturbed quantities, respectively. The magnetic field is written as

$$\boldsymbol{B} = \boldsymbol{B}_{\mathrm{eq}} + \tilde{\boldsymbol{B}}, \tag{4}$$

where $\boldsymbol{B}_{\mathrm{eq}}$ and $\tilde{\boldsymbol{B}}$ defined as

$$\boldsymbol{B}_{\mathrm{eq}} = z + z \times \nabla \Psi_{\mathrm{eq}} \quad \text{and} \quad \tilde{\boldsymbol{B}} = z \times \nabla \tilde{\Psi}, \tag{5}$$

respectively. Here, z denotes the unit vector in the z direction.

In the equilibrium including static islands, equilibrium quantities have the dependence of not only r but also θ and z. We express the equilibrium quantity Q_{eq} with the sum of the symmetric and the island parts, which are referred by the subscripts of 'sym' and 'J', respectively, as follows:

$$Q_{\mathrm{eq}}(r, \theta, z) = Q_{\mathrm{sym}}(r) + Q_J(r, \theta, z). \tag{6}$$

The island part Q_J is expanded into the Fourier series as

$$Q_J(r, \theta, z) = \sum_{n=0, m=n}^{N_{\mathrm{eq}}} \hat{Q}_{J\,m,n}(r) \cos(m\theta - nz), \tag{7}$$

where '$\wedge$' means the Fourier coefficients and N_{eq} denotes the highest mode number in the equilibrium expansion. Since we treat the static island with a single mode of $(m, n) = (1, 1)$, only the components with $n/m = 1$ are picked up in Eq. (7). In the equilibrium poloidal flux, the boundary condition corresponding to the $(m, n) = (1, 1)$ static magnetic islands,

$$\hat{\Psi}_{J\,1,1}(r = 1) = \Psi_b, \tag{8}$$

is imposed as in Refs. [4–6]. Here, Ψ_b is the external poloidal flux at $r = 1$.

The current density in the z direction Jz is expressed as

$$Jz = Jz_{\mathrm{eq}} + \tilde{J}z, \tag{9}$$

where Jz_{eq} and $\tilde{J}z$ are defined as

$$Jz_{\mathrm{eq}} = \nabla_{\perp}^2 \Psi_J \quad \text{and} \quad \tilde{J}z = \nabla_{\perp}^2 \tilde{\Psi}, \tag{10}$$

respectively. The operator $\nabla_{\perp}^2$ is given by

$$\nabla_\perp^2 = \frac{1}{r}\frac{\partial}{\partial r}r\frac{\partial}{\partial r} + \frac{1}{r^2}\frac{\partial^2}{\partial\theta^2}. \tag{11}$$

The vorticity in the negative z direction $\tilde{U}(r,\theta,z)$ is defined as

$$\tilde{U} = \nabla_\perp^2\tilde{\Phi}. \tag{12}$$

The time derivative is given by

$$\frac{d}{dt} = \frac{\partial}{\partial t} + \nabla\Phi\times z\cdot\nabla. \tag{13}$$

The rotational transform ι is defined as

$$\iota(r) = \iota_{\mathrm{sym}}(r) + \iota_J(r), \tag{14}$$

where

$$\iota_{\mathrm{sym}}(r) = \frac{1}{r}\frac{d\Psi_{\mathrm{sym}}(r)}{dr} \quad\text{and}\quad \iota_J(r) = \frac{1}{r}\frac{d\hat{\Psi}_{J\,0,0}(r)}{dr}. \tag{15}$$

In stellarators, the currents in the helical coils generate helical field lines. Since we assume a straight heliotron configuration, the averaged curvature of the field lines $\nabla\Omega$ is given by

$$\frac{d\Omega}{dr} = \frac{N_t\epsilon^2}{l}\frac{1}{r^2}\frac{d}{dr}(r^4\iota_{\mathrm{sym}}). \tag{16}$$

Here, N_t, l and ϵ are the toroidal period number, the pole number and the aspect ratio, respectively. In the case of positive shear of ι_{sym}, $d\Omega/dr$ is positive. The positive $d\Omega/dr$ implies the bad curvature and drives an interchange mode combined with negative dp/dr. Note that this component given by Eq. (16) does not appear in tokamaks without helical coils. The factors S, ν, $\kappa_\perp$ and $\kappa_\parallel$ are the magnetic Reynolds number, the viscosity coefficient, the perpendicular and the parallel heat diffusion coefficients, respectively.

We assume that the perturbed quantities also have a single helicity with $n/m = 1/1$. Under the assumption, we expand the perturbed quantities in the Fourier series as follows :

$$\tilde{\Psi}(r,\theta,z) = \sum_{n=0,m=n}^{N_{\mathrm{pe}}} \tilde{\Psi}_{m,n},$$

$$\tilde{\Psi}_{m,n} = \hat{\Psi}_{m,n}(r)\cos(m\theta - nz), \tag{17}$$

$$\tilde{\Phi}(r,\theta,z) = \sum_{n=0,m=n}^{N_{\mathrm{pe}}} \tilde{\Phi}_{m,n},$$

$$\tilde{\Phi}_{m,n} = \hat{\Phi}_{m,n}(r)\sin(m\theta - nz), \tag{18}$$

$$\tilde{P}(r,\theta,z) = \sum_{n=0,m=n}^{N_{\mathrm{pe}}} \tilde{P}_{m,n},$$

$$\tilde{P}_{m,n} = \hat{P}_{m,n}(r)\cos(m\theta - nz). \tag{19}$$

Here, N_{pe} is the highest mode number for the perturbations. The growth rate is given by

$$\gamma = \frac{1}{2}\frac{1}{E_{\mathrm{K}}}\frac{dE_{\mathrm{K}}}{dt}, \tag{20}$$

where the kinetic energy E_{K} is defined as

$$E_{\mathrm{K}} = \sum_{n=0,m=n}^{N} E_{\mathrm{K}}^{m,n}, \quad E_{\mathrm{K}}^{m,n} = \frac{1}{2}\int |\nabla\tilde{\Phi}_{m,n}\times z|^2 dV. \tag{21}$$

Here, $\int dV$ denotes the integral over the plasma volume.

3. Island Effect on Linear Stability

The MHD equilibria including the static magnetic island with the mode numbers of $(m,n) = (1,1)$ in a straight heliotron configuration are calculated with the FLEC code [13]. The magnetic configuration parameters of $N_t = 10$, $l = 2$ and $\epsilon = 0.16$ are employed in the calculation, which correspond to the LHD configuration. A monotonously increasing rotational transform with $\iota(0) = 0.4$ and $\iota(1) = 1.8$ is also employed. Figure 1 shows the magnetic surfaces and the pressure contour of an example of the equilibria including the static island. The equilibrium corresponds to $w_i = +7.9\times10^{-2}$ or $\Psi_b = +5.0\times10^{-4}$, where w_i is the equilibrium island width normalized by the plasma radius. The magnetic surfaces are plotted by tracing the field lines as explained in Ref. [14]. Figure 2 shows the equilibrium pressure profile along the line connecting the points of $(r = 1, \theta = 0, z = 0)$ and $(r = 1, \theta = \pi, z = 0)$ and the bird's eye view of the profile for $w_i = +7.9\times10^{-2}$ ($\Psi_b = +5.0\times10^{-4}$). The central beta value of 1.5% and the profile of $P_{\mathrm{sym}} = P_0(1 - r^4)$ are assumed in this case. The pressure profile is locally flat inside the separatrix, while the gradient is finite at the X-point and the same as that of P_{sym}. The equilibrium island width varies from -10.4×10^{-2} to $+10.4\times10^{-2}$ for the change of the boundary poloidal flux from $\Psi_b = -1.0\times10^{-3}$ to $+1.0\times10^{-3}$, as shown in Fig. 3. It is noted that positive and negative values correspond to the islands with the O-point located at $\theta = \pi$ and $\theta = 0$, respectively, in this figure.

The NORM code solves the reduced MHD equations as an initial value problem. For each initial component of the perturbations, $\hat{X}_{m,n} = (\hat{\Psi}_{m,n}, \hat{\Phi}_{m,n}, \hat{P}_{m,n})$, we employ the form of

$$\hat{X}_{m,n} = \sigma f(r), \tag{22}$$

where σ denotes the sign which takes the value of $+1$ or -1 and $f(r)$ is a function with a small absolute value corresponding to a white noise. In this study, we utilize the form of $f(r) = 10^{-18}\{1 - 4(r - 1/2)^2\}^2$. The validity of the choice of the initial condition is confirmed by the appearance of the sufficiently long linear phase and the behavior of the nonlinear coupling in Fig. 4. The dissipation parameters of $S = 10^4$, $\nu = 8.5\times10^{-6}$, $\kappa_\perp = 2.0\times10^{-5}$ and $\kappa_\parallel = 2.0$ are used. This choice of these parameters guarantees the $(m,n) = (1,1)$ component is dominant in the time evolution of the mode as discussed later. As the highest Fourier mode numbers, $N_{\mathrm{eq}} = 15$ and $N_{\mathrm{pe}} = 30$ are employed.
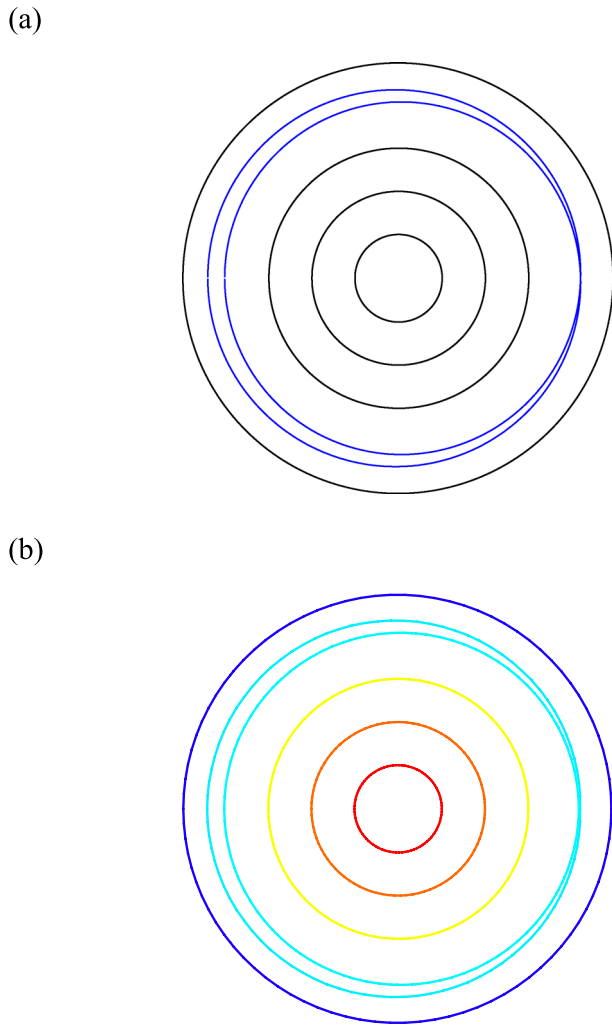
(a)

(a)

(b)

(b)

Fig. 1   (a) Magnetic surfaces and (b) contour of constant pressure of the equilibrium including a static island with the mode number of $(m, n) = (1, 1)$ for $w_i = +7.9 \times 10^{-2}$ ($\Psi_b = +5.0 \times 10^{-4}$). Blue lines show the separatrix of the island.
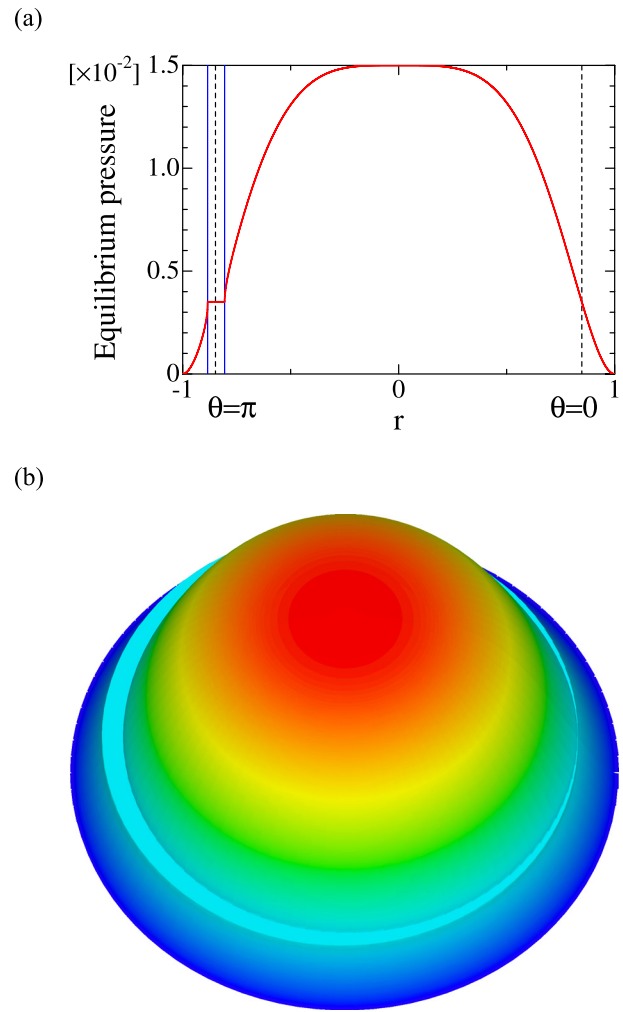
Fig. 2   (a) Equilibrium pressure profile for $w_i = +7.9 \times 10^{-2}$ ($\Psi_b = +5.0 \times 10^{-4}$) and $\beta_0 = 1.5\%$. Blue and dashed lines indicate the positions of the separatrix of the island at $\theta = \pi$ and the positions of the rational surface, respectively. (b) Bird's eye view of the pressure profile.

We discuss the effect of the equilibrium island on the linear stability firstly. Figure 4 shows time evolutions of the kinetic energy for the equilibria without the island corresponding to $w_i = 0$ ($\Psi_b = 0$) and $\sigma = +1$ and with the island corresponding to $w_i = +2.8 \times 10^{-2}$ ($\Psi_b = +5.0 \times 10^{-5}$) and $\sigma = +1$. The linear phase appears in the whole range of $\Psi_b = -1.0 \times 10^{-3}$ to $+1.0 \times 10^{-3}$, where the $(m, n) = (1, 1)$ component is dominant. The relation of the linear growth rates among the components is different between the cases with $w_i = 0$ and $w_i \neq 0$. The growth rate of $E_K^{n,n}$ increases as the mode number becomes large in the case of $w_i = 0$, while the growth rate of each mode number is almost the same in the case of $w_i \neq 0$. As is explained in Ref. [7], this feature for $w_i \neq 0$ is attributed to the fact that the $(m, n) = (1, 1)$ component is dominant and the relation of $|\hat{\Psi}_{J\ 1,1}| \gg |\hat{\Psi}_{1,1}|$ is satisfied in the linear phase.

Figure 5 shows the dependence of the growth rate

γ on w_i. The growth rate γ is decreased as w_i is increased, and the interchange mode is completely stabilized when w_i exceeds a threshold value. The threshold island width for the marginal stability is $|w_i| = 5.7 \times 10^{-2}$ ($|\Psi_b| = 2.3 \times 10^{-4}$) in the present case. In the decrease of the growth rate, the mode structure of the stream function $\hat{\Phi}_{1,1}$ hardly changes as shown in Fig. 6. The half-width of the mode w_H is 6.5×10^{-2} for $w_i = 0$ ($\Psi_b = 0$) and 6.6×10^{-2} for $w_i = +4.6 \times 10^{-2}$ ($\Psi_b = +1.5 \times 10^{-4}$). Therefore, the threshold island width is 0.88 of w_H of the stream function for $w_i = 0$ ($\Psi_b = 0$). When σ is changed, the sign of the eigenfunctions becomes opposite while the growth rate is the same. This linear stability dependence on w_i implies that the static magnetic islands have a stabilizing contribution to the interchange mode. The driving force of the interchange mode is reduced by the local flattening of the pressure profile at the resonant surface, because the mode is driven by the pressure gradient and the field line curva-
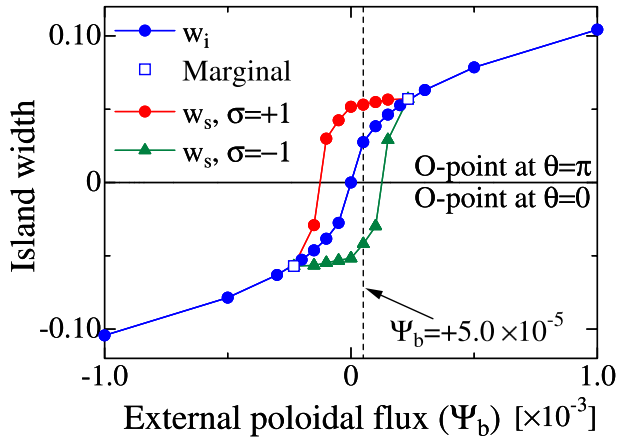
Fig. 3 Dependence of island width on Ψ_b. Positive and negative values correspond to the island with the O-point at $\theta = \pi$ and $\theta = 0$, respectively. Blue circles and squares show w_i and the threshold width for the marginal stability, respectively. Red circles and green triangles show the island width in the saturation of interchange modes, w_s, for $\sigma = +1$ and $\sigma = -1$, respectively.
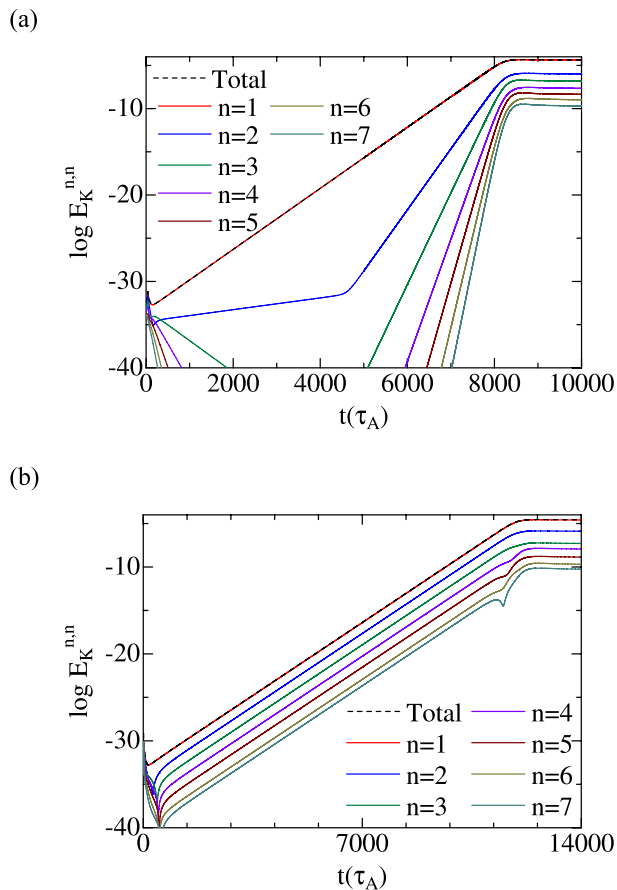
(a)

(b)

Fig. 4 Time evolution of the kinetic energy for (a) $w_i = 0$ ($\Psi_b = 0$) and $\sigma = +1$ and (b) $w_i = +2.8 \times 10^{-2}$ ($\Psi_b = +5.0 \times 10^{-5}$) and $\sigma = +1$.
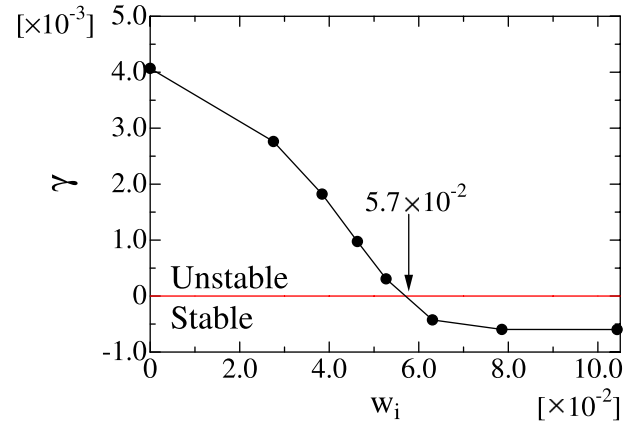

Fig. 5 Dependence of the growth rate of the interchange mode in the linear phase on w_i.
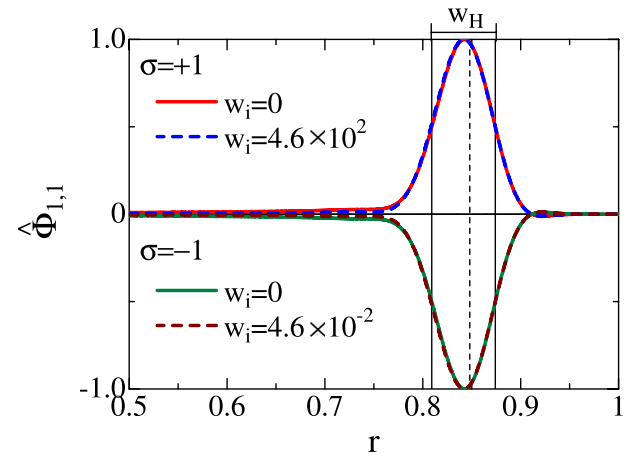

Fig. 6 Normalized $\hat{\Phi}_{1,1}$ for $w_i = 0$ ($\Psi_b = 0$) and $w_i = +4.6 \times 10^{-2}$ ($\Psi_b = +1.5 \times 10^{-4}$). Dashed line indicates the position of the rational surface. Vertical black solid lines indicate the positions corresponding to the half value of the normalized $\hat{\Phi}_{1,1}$ for $\Psi_b = 0$.

ture. It is already obtained for the case of the annular structure of the flat region that the growth rate is reduced with the increase of the width of the flat region. A quarter of the half-width of the stream function obtained without the flat region is needed for the complete stabilization in this annular case [16]. In the present analysis, the flat width in the pressure profile is not constant in the poloidal direction. The width is maximum at the O-point, while the original finite pressure gradient remains at the X-point as shown in Fig. 2. Even in this case, the pressure flattening in the separatrix stabilizes the interchange mode. Comparing with the annularly flat case, the threshold width in the static island case is larger than that in the annularly flat case. This is due to the fact that the stabilizing effect of the static island is weakened by the decrease of the flat width from the O-point to the X-point and the existence of the finite gradient X-point.

4. Nonlinear Interaction between Static Magnetic Islands and Resistive Interchange Modes

As shown in Fig. 4, a steady state appears after the linear phase in the time evolution of the interchange mode when the mode is unstable. Thus, we discuss the behavior of the interchange mode and the changes of the island width and the pressure profile in the nonlinear steady state. The steady state is identified with the condition of $|\gamma| < 10^{-5}$. Figure 7 (a) shows the dependence of the total kinetic energy E_K in the steady state on w_i. As w_i is increased, E_K is decreased. This dependence is similar to that of the linear growth rate shown in Fig. 5. That is, the slow growth of the mode leads to a low saturation level. Figure 7 (b) shows the profile of $\hat{\Phi}_{1,1}$ in the steady state. As w_i is increased, the absolute value of $\hat{\Phi}_{1,1}$ is decreased, while the half-width is almost constant for w_i. Therefore, the decrease of E_K in the steady state is attributed to the decrease of the absolute value of $\hat{\Phi}_{1,1}$. This tendency seems to be consistent with the experiment [2] that the fluctuation amplitude is decreased with the increase of the RMP.
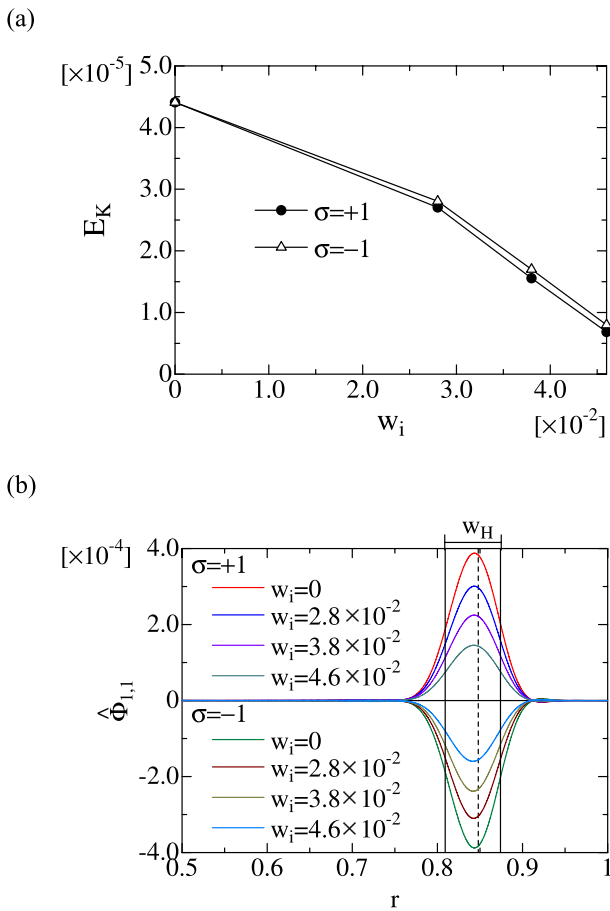
We analyze the behavior of the island due to the nonlinear evolution of the interchange mode. Before the discussion for the case of the finite w_i, we examine the change of the magnetic island in the case of $w_i = 0$ ($\Psi_b = 0$) as a reference. Figure 8 (a) shows the magnetic surfaces for $w_i = 0$ ($\Psi_b = 0$) and $\sigma = +1$ at $t = 10000\tau_A$. Since we employ a large resistivity of $S = 10^4$ in the present analysis, the interchange mode generates a magnetic island with a substantial width even in the case of $w_i = 0$. In the present choice of the dissipation parameters, there are two O-points at $\theta = 0$ and $\theta = \pi$, which are shown by the green and the blue lines, respectively. That is, the separatrix is composed of the mixed islands of the $m = 1$ and the $m = 2$ components. However, the island width with the O-point located at $\theta = \pi$ is $+5.2 \times 10^{-2}$ and the other is -5.8×10^{-3}. Therefore, the island with the O-point located at $\theta = \pi$ is much larger than that with the O-point located at $\theta = 0$. This means that the $m = 1$ island is dominant. Thus, we neglect the smaller island and regard the separatrix as the $m = 1$ island. And hereafter, we refer the O-point of the

(a)

(b)

Fig. 7 (a) Dependence of the kinetic energy on w_i, and (b) profiles of $\hat{\Phi}_{1,1}$ in the steady state. Vertical black solid lines indicate the positions corresponding to the half value of $\hat{\Phi}_{1,1}$ in the steady state for $w_i = 0$.
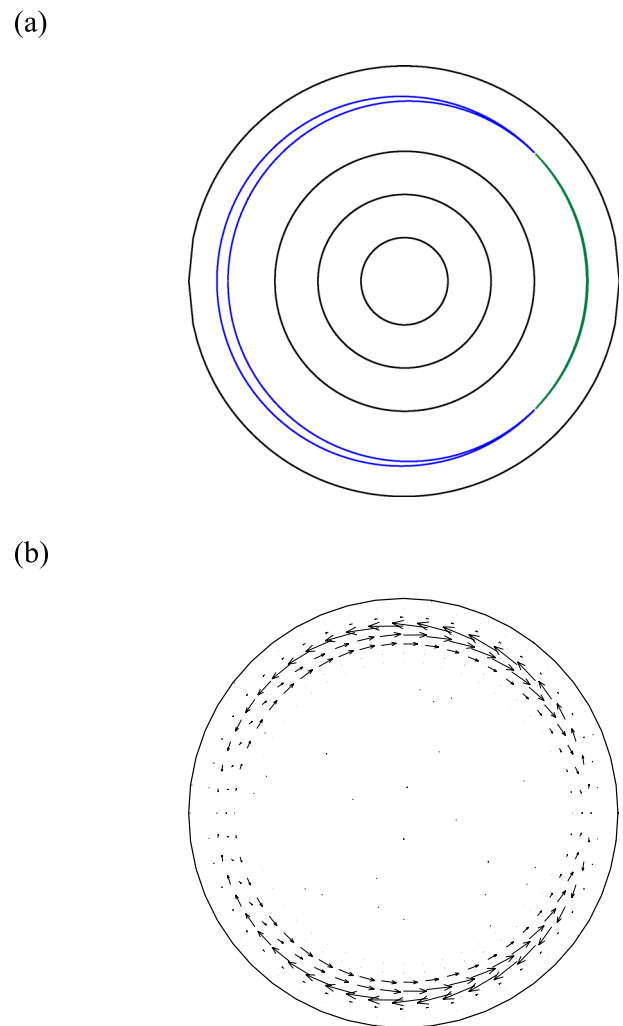
(a)

(b)

Fig. 8 (a) Magnetic surfaces and (b) flow pattern at $t = 10000\tau_A$ for $w_i = 0$ ($\Psi_b = 0$) and $\sigma = +1$.

smaller island as the X-point of the larger island. The flow pattern of the vortex calculated from $\tilde{\Phi}$ at $t = 10000\tau_A$ is also plotted in Fig. 8 (b). This flow shows a typical pattern of an $m = 1$ interchange mode. The influence of the $m = 2$ component to the flow is too small to be recognized. Thus, the flow pattern also validates the neglect of the $m = 2$ component. There exist the outward and the inward radial flows at the X-point of $\theta = 0$ and the O-point of $\theta = \pi$, respectively. The directions of the flow is consistent with the reconnection at the X-point. In the case of $\sigma = -1$, the phase of the magnetic surfaces and the flow are opposite to those of $\sigma = +1$.

Next, we discuss the case of $w_i \neq 0$ ($\Psi_b \neq 0$). The magnetic surfaces at $t = 0$ and $t = 14000\tau_A$ are shown in Figs. 9 and 10. The separatrix is composed of the mixed islands of the $m = 1$ and the $m = 2$ components in the magnetic surfaces at $t = 14000$ in both cases as in the case of $w_i = 0$. We also neglect the $m = 2$ component and regard the separatrix as the $m = 1$ island. In the case of $w_i = +2.8 \times 10^{-2}$ ($\Psi_b = +5.0 \times 10^{-5}$) and $\sigma = +1$, the island width is increased by the nonlinear evolution of the interchange mode as shown in Fig. 9. In the case of $w_i = +2.8 \times 10^{-2}$ ($\Psi_b = +5.0 \times 10^{-5}$) and $\sigma = -1$, the island phase is changed by the interchange mode as shown in Fig. 10.

The island width in the steady state, w_s, is summarized in Fig. 3. Red circles and green triangles show the width for $\sigma = +1$ and $\sigma = -1$, respectively. Blue squares show the threshold width for the marginal stability ($w_i = +5.7 \times 10^{-2}$). The island width changes only in the region of $|w_i| \leq 5.7 \times 10^{-2}$, because the interchange mode is stable outside the region. In the region $|w_i| < 5.7 \times 10^{-2}$, there are two cases in the island change depending on σ. One is the increase of the island width and the other is the decrease of the width as in the study of Ref. [7]. In the latter case, the island phase can also be changed. Figures 9 and 10 are the examples of the former and the latter changes, respectively. These changes are attributed to the fact that the island width in the steady state is determined by the superposition of the island generated by the nonlinear evolution of the interchange mode and the equilibrium magnetic island. The island width is increased if the phase of the equilibrium island is the same as that of the island generated by the interchange mode, and decreased if opposite. The phase of the island generated by the interchange mode depends on σ. Therefore, the two kinds of change in the island width occur depending on σ. The flow patterns of the two cases are also plotted in Fig. 9 (c) and Fig. 10 (c). The island width increases when the flow direction is radially outward at the X-point of the equilibrium island. The island width decreases and the island phase can change when the flow direction is radially inward at the X-point. The radially outward shift of the plasma compresses the magnetic surfaces, which enhances the reconnection of the field lines. Therefore, the radial direction of the flow is consistent with the driven reconnection of the field lines.
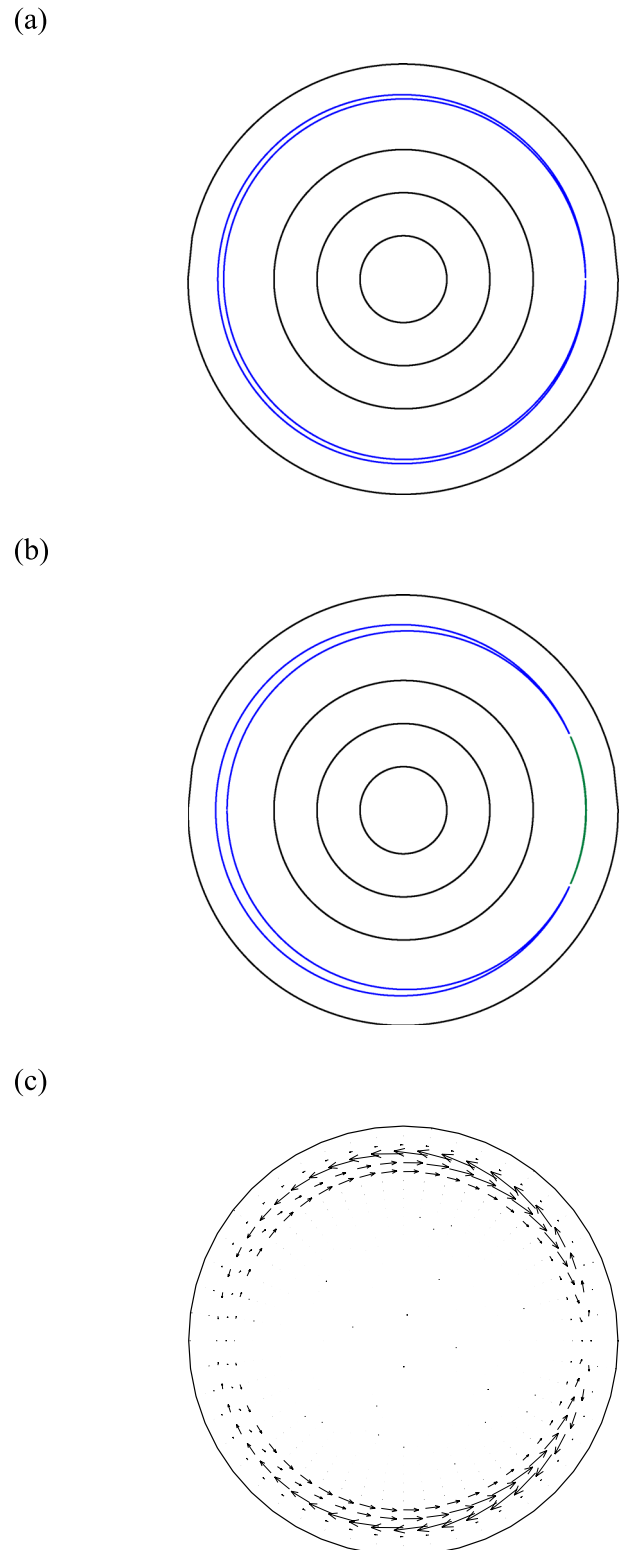
(a)

(b)

(c)

Fig. 9   Magnetic surfaces at (a) $t = 0$ and (b) $t = 14000\tau_A$ and (c) flow pattern at $t = 14000\tau_A$ for $w_i = +2.8 \times 10^{-2}$ ($\Psi_b = +5.0 \times 10^{-5}$) and $\sigma = +1$.

The nonlinear saturation of the interchange mode also deforms the pressure profile. Figure 11 shows the pressure profiles along the line connecting the points of ($r = 1, \theta =$
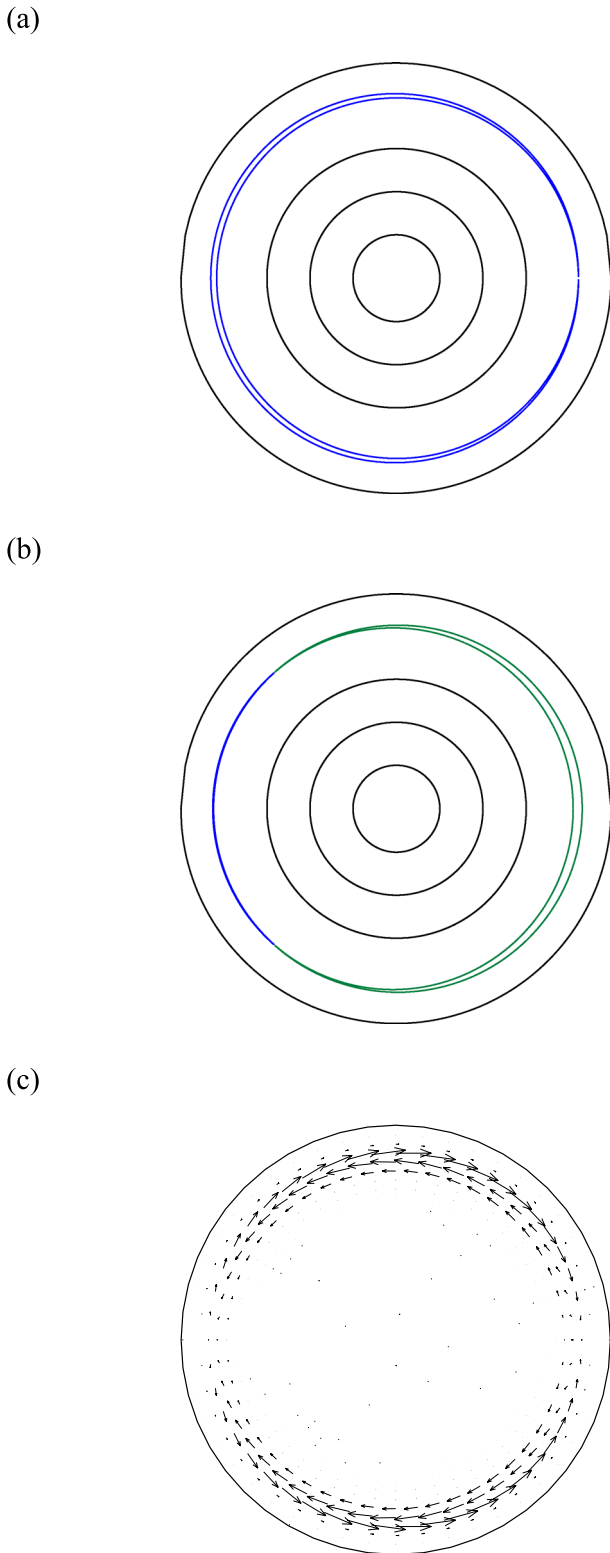
(a)

(b)

(c)

Fig. 10   Magnetic surfaces at (a) $t = 0$ and (b) $t = 14000\tau_A$ and (c) flow pattern at $t = 14000\tau_A$ for $w_i = +2.8 \times 10^{-2}$ ($\Psi_b = +5.0 \times 10^{-5}$) and $\sigma = -1$.

(a)

(b)

(c)

Fig. 11   Profiles of pressure (a) along the line connecting ($r = 1, \theta = 0, z = 0$) and ($r = 1, \theta = \pi, z = 0$) and the enlargements at (b) $\theta = 0$ and (c) $\theta = \pi$ for $w_i = 0$ ($\Psi_b = 0$) and $\sigma = \pm1$. Black solid lines show the equilibrium pressure profile. Red and green solid lines show the pressure profiles in the steady state ($t = 10000\tau_A$) for $\sigma = +1$ and $\sigma = -1$, respectively. Vertical dashed lines indicate the positions of the rational surface.

$0, z = 0$) and ($r = 1, \theta = \pi, z = 0$) at $t = 0$ and $t = 10000\tau_A$ for $w_i = 0$ ($\Psi_b = 0$) and $\sigma = \pm1$. The $m = 1$ deformation due to the interchange mode around the resonant surface
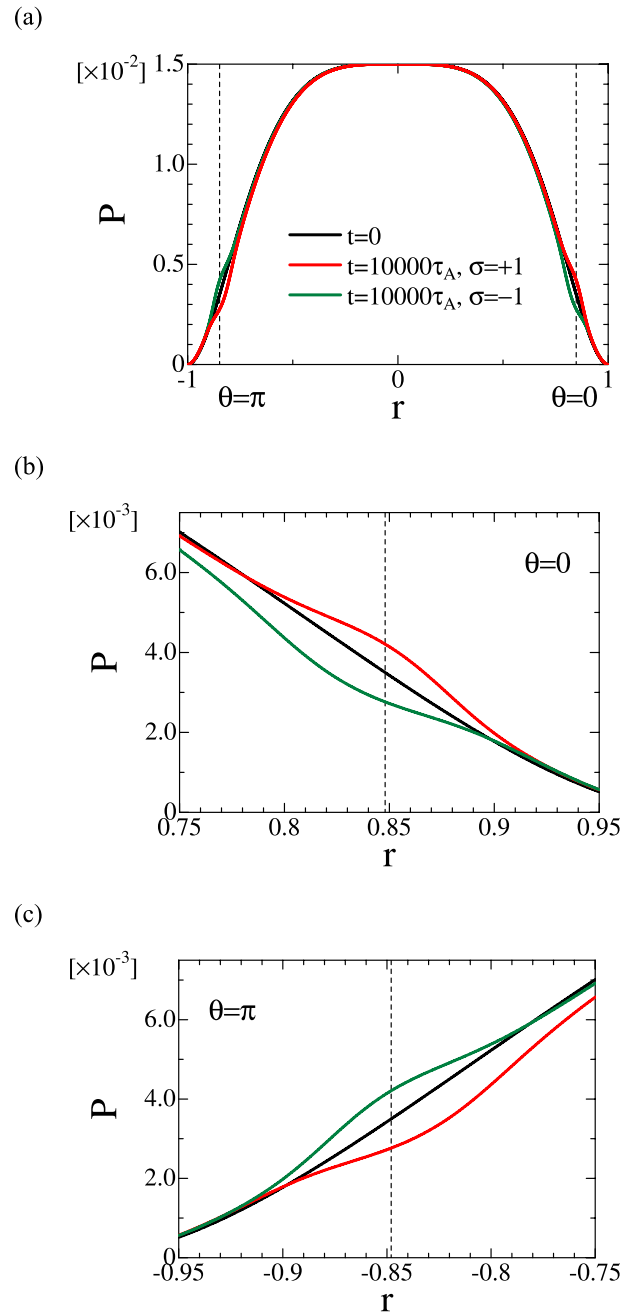
with $t = 1$ is seen. This deformation is generated by the convection of the radial flow. The flow direction is radially outward at $\theta = 0$ and inward at $\theta = \pi$ for $\sigma = +1$ as shown in Fig. 8. Therefore, the plasma with the higher pressure at the inside of the rational surface is convected to the outside of the surface at $\theta = 0$, and the plasma with the
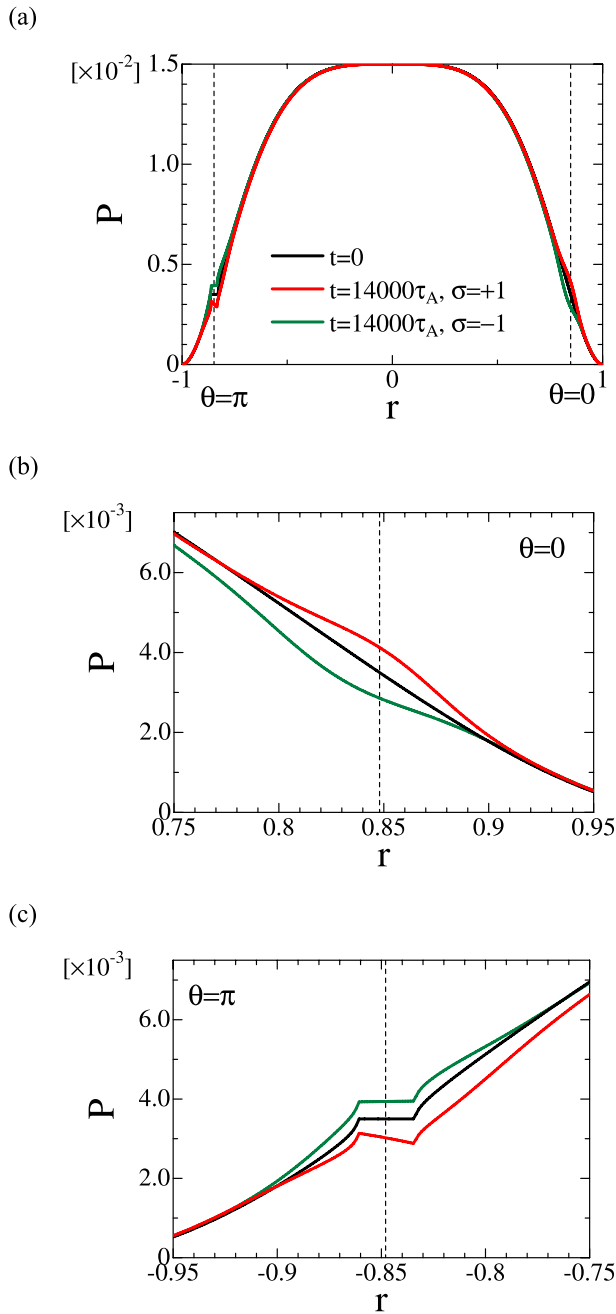
(a)

(b)

(c)

Fig. 12 Profiles of pressure (a) along the line connecting ($r = 1, \theta = 0, z = 0$) and ($r = 1, \theta = \pi, z = 0$) and the enlargements at (b) $\theta = 0$ and (c) $\theta = \pi$ for $w_i = +2.8 \times 10^{-2}$ ($\Psi_b = +5.0 \times 10^{-5}$) and $\sigma = \pm 1$. Black solid lines show the equilibrium pressure profile. Red and green solid lines show the pressure profiles in the steady state ($t = 14000\tau_A$) for $\sigma = +1$ and $\sigma = -1$, respectively. Vertical dashed lines indicate the positions of the rational surface.

lower pressure at the outside of the surface is convected to the inside of the surface at $\theta = \pi$. As a result, the pressure is increased at the X-point of the generated island and decreased at the O-point. This mechanism is the same for $\sigma = -1$.

This mechanism is also the same in the finite w_i case.

Figure 12 shows the pressure profiles for $w_i = +2.8 \times 10^{-2}$ ($\Psi_b = +5.0 \times 10^{-5}$) and $\sigma = \pm 1$. The change of the pressure is due to the convection of the radial flow as in the case of $w_i = 0$. It is remarkable that the local flat structure at the O-point of the equilibrium island or at $\theta = \pi$ remains even in the saturation phase in either value of σ. Particularly, in the case of $\sigma = -1$, the pressure is increased at $\theta = \pi$ with the local flat structure kept in spite of the fact that the point is changed to the X-point from the O-point as shown in Fig. 10. Therefore, the nonlinear saturation of the interchange mode does not reproduce a new equilibrium with a pressure profile corresponding to the resultant magnetic islands.

5. Conclusions

The effects of the $(m, n) = (1, 1)$ static magnetic island on the resistive interchange mode with the same mode number are studied. For this purpose, we utilize equilibria with the pressure profile consistent with the island geometry of which the gradient at the X-point is finite. The linear growth rate of the interchange mode is reduced by the equilibrium island in spite of the finite pressure gradient at the X-point. Beyond a threshold island width, the mode is completely stabilized. The threshold width is almost the same as the half-width of the stream function obtained for the equilibrium without the island. The effect of the static island on the interchange mode can be observed in RMP experiments by detecting both the width of the flat region in the pressure profile data and the fluctuation amplitude resonant at the surface of the island. The stabilizing tendency and the existence of the threshold width obtained in the present analysis is consistent with the experimental results in LHD [2]. More quantitative comparison will be planed in future.

In the nonlinear saturation phase of the unstable interchange mode, the saturation level of the kinetic energy is also decreased as the island width is increased. On the other hand, the nonlinear evolution changes the shape of the magnetic island. If the phase of the equilibrium island is the same as that of the island generated by the interchange mode, the island width is increased. If the phase is opposite, the island width is decreased and the phase can also be changed. In the point of the relation with the flow generated by the mode, the island width increases when the flow direction is radially outward at the X-point of the initial static island and decreases when the flow direction is radially inward at the X-point. The interchange mode also changes the pressure profile through the convection. The tendency of the profile change is almost independent of the equilibrium island structure. The pressure is increased and decreased by the outward and the inward flows, respectively. The local flat structure at the O-point of the static island is almost kept even if this point is changed to the X-point.

One of the future works is the incorporation of the uni-

form poloidal flow such as a diamagnetic flow. If the effect is included, the interchange modes are possible to rotate. Then, the static island with a substantial width may lock the mode rotation. Such mode locking was discussed in Ref. [9] with a smooth equilibrium pressure profile. By utilizing the local flat equilibrium pressure consistent with the island structure, the mode locking due to the static island can be investigated more consistently.

Another future work is the change of the Fourier mode of the perturbation. In the present analysis, we focus on the interaction between the static island and the interchange mode with the same mode numbers, $(m, n) = (1, 1)$. For this purpose, we adjust the dissipation parameters so that the $(1, 1)$ component of the interchange mode should be dominant. By choosing appropriate dissipation parameters, we can set the dominant mode numbers to higher numbers, such as $(2, 2)$, $(3, 3)$ and so on. It is interesting to analyze the change of the $(1, 1)$ island structure due to the dynamics flow with such high mode numbers. On the other hand, the interaction between the islands with higher mode numbers of $(2, 2)$, $(3, 3)$ and so on and the $(1, 1)$ interchange mode is considered as another research aspect. Also in this case, the islands make the equilibrium pressure profile locally flat. Therefore, it is expected that the islands essentially have a stabilizing contribution to the interchange mode as well. However, further calculations are needed to obtain the quantitative stabilizing property.

Including the multi-helicity perturbation should also be considered. Local flattening of the pressure profile makes the pressure gradient steeper in the region just outside the separatrix. Therefore, the interchange mode resonant at the region can be destabilized. Since such a mode has a helicity different from that of the static island, the multi-helicity perturbations are needed to analyze the effect of the static island on the interchange stability in the whole plasma.

Acknowledgments

[1] M.E. Fenstermacher, M. Becoulet, P. Cahyna, J. Canik, C.S. Chang, T.E. Evans, P. Gohli, S. Kaye, A. Kirk, Y. Liang, A. Loarte, R. Maingi, O. Shmitz, W. Suttrop and H.R. Wilson, Proceedings of 23rd IAEA Fusion Energy Conference, 11-16 October 2010, Daejeon, Republic of Korea, ITR/P1-30.

[2] H. Yamada, K.Y. Watanabe, S. Sakakibara, Y. Suzuki, S. Ohdachi, M. Kobayashi, H. Funaba and the LHD Experimental Group, Contrib. Plasma Phys. **50**, No.6-7, 480 (2010).

[3] A. Komori, H. Yamada, O. Kaneko, K. Kawahata, T. Mutoh, N. Ohyabu, S. Imagawa, K. Ida, Y. Nagayama, T. Shimozuma, K.Y. Watanabe, T. Mito, M. Kobayashi, K. Nagaoka, R. Sakamoto, N. Yoshida, S. Ohdachi, S. Sakakibara, N. Ashikawa, Y. Feng, T. Fukuda, H. Igami, S. Inagaki, H. Kasahara, S. Kubo, R. Kumazawa, O. Mitarai, S. Murakami, Y. Nakamura, M. Nishiura, T. Hino, S. Masuzaki, K. Tanaka, K. Toi, A. Weller, M. Yoshinuma, Y. Narushima, N. Ohno, T. Okamura, N. Tamura, K. Saito, T. Seki, S. Sudo, H. Tanaka, T. Tokuzawa, N. Yanagi, M. Yokoyama, Y. Yoshimura, T. Akiyama, H. Chikaraishi, M. Chowdhuri, M. Emoto, N. Ezumi, H. Funaba, L. Garcia, P. Goncharov, M. Goto, K. Ichiguchi, M. Ichimura, H. Idei, T. Ido, S. Iio, K. Ikeda, M. Irie, A. Isayama, T. Ishigooka, M. Isobe, T. Ito, K. Itoh, A. Iwamae, S. Hamaguchi, K. Hamajima, S. Kitajima, S. Kado, D. Kato, T. Kato, S. Kobayashi, K. Kondo, S. Masamune, H. Matsumoto, N. Matsunami, T. Minami, C. Michael, H. Miura, J. Miyazawa, N. Mizuguchi, T. Morisaki, S. Morita, G. Motojima, I. Murakami, S. Muto, K. Nagasaki, N. Nakajima, Y. Nakamura, H. Nakanishi, H. Nakano, K. Narihara, A. Nishimura, H. Nishimura, K. Nishimura, S. Nishimura, N. Nishino, T. Notake, T. Obana, K. Ogawa, Y. Oka, T. Ohishi, H. Okada, K. Okuno, K. Ono, M. Osakabe, T. Osako, T. Ozaki, B.J. Peterson, H. Sakaue, M. Sasao, S. Satake, K. Sato, M. Sato, A. Shimizu, M. Shiratani, M. Shoji, H. Sugama, C. Suzuki, Y. Suzuki, K. Takahata, H. Takahashi, Y. Takase, Y. Takeiri, H. Takenaga, S. Toda, Y. Todo, M. Tokitani, H. Tsuchiya, K. Tsumori, S. Urano, E. Veshchev, F. Watanabe, T. Watanabe, T.H. Watanabe, I. Yamada, S. Yamada, O. Yamagishi, S. Yamaguchi, S. Yoshimura, T. Yoshinaga and O. Motojima, Proceedings of the 22nd Fusion Energy Conference OV/2-4 (2008).

[4] T. Unemura, S. Hamaguchi and M. Wakatani, Phys. Plasmas **11**, 1545 (2004).

[5] L. Garcia, B.A. Carreras, V.E. Lynch, M.A. Pedrosa and C. Hidalgo, Phys. Plasmas **8**, 4111 (2001).

[6] L. Garcia, B.A. Carreras, V.E. Lynch and M. Wakatani, Nucl. Fusion **43**, 553 (2003).

[7] K. Saito, K. Ichiguchi and N. Ohyabu, Phys. Plasmas **17**, 062504 (2010).

[8] K. Saito, K. Ichiguchi and R. Ishizaki, Plasma Fusion Res. **6**, 2403072 (2011).

[9] S. Nishimura, K. Itoh, M. Yagi, K. Ida and S.-I. Itoh, Phys. Plasmas **17**, 122505 (2010).

[10] S. Nishimura and M. Yagi, Plasma Fusion Res. **6**, 2403119 (2011).

[11] S. Nishimura, S. Toda, Y. Narushima and M. Yagi, Plasma Phys. Control. Fusion, in press, (2012).

[12] H.R. Strauss, Plasma Phys. **22**, 733 (1980).

[13] K. Saito, K. Ichiguchi and R. Ishizaki, Plasma Fusion Res. **7**, 1403070 (2012).

[14] K. Saito, K. Ichiguchi and R. Ishizaki, Plasma Fusion Res. **7**, 2403032 (2012).

[15] K. Ichiguchi, N. Nakajima, M. Okamoto, N. Ohyabu, T. Tatsuno, M. Wakatani and B.A. Carreras, J. Plasma Fusion Res. SERIES **2**, 286 (1999).

[16] K. Ichiguchi, M. Wakatani, T. Unemura, T. Tatsuno and B.A. Carreras, Nucl. Fusion **41**, 181 (2001).

[17] K. Ichiguchi, N. Nakajima, M. Wakatani, B.A. Carreras and V.E. Lynch, Nucl. Fusion **43**, 1101 (2003).